NUMERICAL FLOOD ROUTING MODELS USED IN NWS

D. L. Fread

Hydrologic Research Laboratory, NWS
Silver Spring, MD 20910

Three numerical dynamic routing models (DWOPER,DAMBRK,SMPDBK) have been developed by the National Weather Service (NWS) to route floods through rivers, reservoirs, and estuaries. The DWOPER model is based on an implicit finite-difference solution of the Saint-Venant one-dimensional equations of unsteady flow, and is suitable for real-time routing of floods through a single waterway (river) or a system of inter-connected waterways. The DAMBRK model (also based on the Saint-Venant equations) and the SMPDBK model (a much simplified version of DAMBRK) are used for real-time forecasting of dam-break floods emanating from breached dams along a single river. These models are also extensively used by many federal and state agencies concerned with dam safety and associated emergency evacuation plans. More recently a new comprehensive flood routing model (FLDWAV) has been undergoing development and testing; it combines the capabilities of the DWOPER and DAMBRK models as well as provides features not contained in either of these models. The FLDWAV model will be placed in operational use in NWS during the next several years. This paper describes the characteristics and capabilities of the four models with emphasis on the new FLDWAV model.

INTRODUCTION

The National Weather Service (NWS) hydrology program provides flood and daily river forecasts to the general public. Thirteen River Forecast Centers prepare the forecasts for dissemination throughout the United States.

Within NWS flood forecasting procedures such as the National Weather Service River Forecast System (NWSRFS), the runoff generated by rainfall-runoff models is aggregated in fairly large, well-defined channels (rivers), and then transmitted downstream by unsteady flow routing techniques of the hydrologic or storage variety. Although these routing techniques function adequately in many locations, they have serious shortcomings when the unsteady flows are subjected to backwater effects due to reservoirs, tides, or inflows from large tributaries. When effective hydraulic slopes of the rivers are quite mild, the flow inertial effects ignored in the hydrologic techniques become important. Also, highly transient flows resulting from dam breaks which usually greatly exceed the flood-of-record are not treated adequately by the hydrologic routing methods.

To improve the routing capabilities within NWS forecasting procedures, the Hydrologic Research Laboratory has developed dynamic routing models suitable for efficient operational use in a wide variety of applications involving the prediction of unsteady flows in rivers, reservoirs, and estuaries.

One of the models, Dyanmic Wave Operational (DWOPER), developed in the early 1970's and enhanced in the early 1980's, is based on an implicit finite-difference solution of the Saint-Venant one-dimensional equations of unsteady flow. The DWOPER model is used for real-time routing of rainfall/snowmelt-

generated floods, hurricane-generated storm surges, tidal fluctuations, and reservoirs releases to a single reach of river or a system of interconnected rivers, such as the Mississippi, Ohio, Columbia, and several Gulf coast rivers. Also, DWOPER has received considerable use by other Government agencies and private consultants in engineering/design studies of waterways.

Catastrophic flooding emanating from breached dams along a single river is forecasted by the Dam-Break (DAMBRK) model (also based on the Saint-Venant equations) and the SMPDBK model (a much simplified dam-break flood forecasting model). DAMBRK, developed in 1977, has been adopted for use in the United States by most federal and state agencies concerned with dam safety and associated emergency evacuation plans. Also, DAMBRK is being used in many other countries around the world by governmental agencies, power companies, and private engineering consultants. Research has been on-going in developing improvements in the DAMBRK model allowing it to have an increasing range of application. The most recent version of DAMBRK became operational in late 1988. DAMBRK can be used also for routing any specified hydrograph through reservoirs, rivers, canals, or estuaries as part of general engineering studies of waterways. Simplified Dam-Break (SMPDBK), developed in 1982-83, has received considerable use within NWS and by other agencies in the United States when available time and resources are too limited for the use of DAMBRK and the attendant reduction in accuracy is judged acceptable. Another NWS model, BREACH, developed in 1984-85, predicts only the breach hydrograph and the breach size and its time of formation due to overtopping or piping of earthen dams that are man-made or naturally formed due to landslide blockages of streams and rivers. It is intended to aid in the selection of breach parameters for DAMBRK and SMPDBK.

More recently a new comprehensive flood routing model Flood Wave (FLDWAV) has been undergoing development and testing; it combines the capabilities of DWOPER and DAMBRK as well as provides features not contained in either of these models. The FLDWAV model will be placed in operational use within NWS during the next several years.

Scope

Since FLDWAV encompasses the features of both the DWOPER and DAMBRK models, it is presented first herein. Then, the DWOPER and DAMBRK models' departures and exceptions to the FLDWAV model are presented. Finally, descriptions of the SMPDBK and BREACH models are given. All models are written in Fortran and suitable for execution on main-frame, mini, or micro-computers; the latter must have 640K storage and a math coprocessor.

FLDWAV MODEL

The FLDWAV model is based on an implicit finite-difference solution of the complete one-dimensional Saint-Venant equations of unsteady flow coupled with an assortment of internal boundary conditions for simulating unsteady flows controlled by a wide spectrum of hydraulic structures. The flow may occur in a single waterway or a system of inter-connected waterways in which sinuosity effects are considered. The flow which can range from Newtonian (water) to non-Newtonian (mud/debris, mine tailings) may freely change with time and location from subcritical to supercritical or vice versa, and from free-surface to pressurized flow. Special modelling features include time-

dependent dam breaches, levee overtopping and crevasse, time-dependent gate controlled flows, assorted spillway flows, bridge/embankments, tidal flap gates, off-line detention basins and/or pumping basins including individual pump specifications, and floodplain compartments with free/submerged weir flow connecting with the waterway or adjacent compartments. FLDWAV can be automatically calibrated for a single channel or dendritic system of channels; calibration is achieved through an efficient automatic adjustment of the Manning coefficient that varies with location and flow depth. The model has automatic selection of the critical computational time and distance steps. Data input is through either a batch or an interactive mode and output is tabular and graphic. Input/output may be in English or metric units. It is planned that future NWS research and development in river mechanics will be integrated within the FLDWAV model frame-work. The model can be used by hydrologists/engineers for a wide range of unsteady flow applications including real-time flood forecasting in a dendritic system of waterways subject to backwater effects; real-time dam-breach flood forecasting or preparation of inundation maps for sunny-day dam-breach piping failures or overtopping failures due to Probable Maximum Flood (PMF) reservoir inflows including the complexities associated with failure of two or more dams sequentially located along a watercourse; design of waterway improvement structures such as levees, off-channel detention ponds, etc.; floodplain mapping for flood insurance studies; analysis of irrigation systems with gate controlled flows; analysis of storm sewer systems having a combination of free surface and/or pressurized unsteady flows; mud/debris flow inundation mapping; and unsteady flows due to hydro-power operations.

Governing Equations

The governing equations of the FLDWAV model are: (1) an expanded form of the one-dimensional equations of unsteady flow originally derived by Saint-Venant (1871); (2) an assortment of internal boundary equations representing flow through one or more hydraulic flow control structures located sequentially along the main-stem river and/or its tributaries (distributaries); and (3) external boundary equations describing known upstream/downstream discharges or water elevations which vary either with time or each other.

The Saint-Venant equations of conservation of mass and momentum may be expressed in an expanded form to account for some effects omitted in their original derivation. These effects are: (1) lateral inflows/outflows, (2) nonuniform velocity distribution across the flow section, (3) expansion/contraction losses, (4) off-channel (dead) storage, (5) flow-path differences between a sinuos channel and its floodplain, (6) surface wind resistance, and (7) internal viscous dissipation of non-newtonian (mud/debris) flows. The conservation of mass (continuity) equation is:

$$\partial Q/\partial x + \partial s_c(A+A_o)/\partial t - q = 0 \qquad (1)$$

in which Q is discharge (flow), A is wetted active cross-sectional area, A_o is wetted inactive off-channel (dead) storage area associated with topographical embayments or tributaries, s_c and s_m are depth-dependent sinuosity coefficients (DeLong, 1985) that account for channel meander, q is lateral flow (inflow is positive, outflow is negative), t is time, and x is distance measured along the mean flow-path of the floodplain or along the channel if there is minimal channel meander. The conservation of momentum equation is:

$$\partial(s_m Q)/\partial t + \partial(\beta Q^2/A)/\partial x + gA(\partial h/\partial x + S_f + S_e + S_i) + L + W_f B = 0 \quad \ldots\ldots\ldots(2)$$

in which g is the gravity acceleration constant; h is the water surface elevation; B is the wetted cross-sectional active topwidth; L is the momentum effect (Strelkoff, 1970) of lateral flows ($L = -qv_x$ for lateral inflow, where v_x is the lateral inflow velocity in the x-direction; $L = -q\,Q/(2A)$ for seepage lateral outflows; $L = -q\,Q/A$ for bulk lateral outflows); W_f is the wind factor (Fread, 1985), i.e., $W_f = C_w|V_r|V_r$ in which C_w is the wind resistance coefficient, and $V_r = Q/A - v_w \cos\omega$, where v_w is the wind velocity and ω is the acute angle between the wind direction and x-axis; S_f is the boundary friction slope, i.e., $S_f = |Q|Q/K^2$ in which K is the total conveyance determined by summing conveyances of the left/right floodplains and channel in which the channel conveyance is modified by the factor $(1/\sqrt{s_m})$ and all conveyances are determined automatically from the data input of topwidth/Manning n versus elevation tables for cross sections of the channel and left/right floodplains; S_e is the expansion/contraction slope, i.e., $S_e = k_e/(2g)\,\partial(Q/A)^2/\partial x$ in which k_e is the expansion/contraction loss coefficient; β is the momentum coefficient for non-uniform velocity distribution and is internally computed from the conveyances and areas associated with flow in the channel and left/right floodplains and S_i is the non-Newtonian internal viscous dissipation slope (Fread, 1987), i.e.,

$$S_i = \kappa/\gamma[(b+2)Q/(AD^{b+1}) + (b+2)/(2D^b)\,(\tau_o/\kappa)^b]^{1/b} \quad \ldots\ldots\ldots(3)$$

in which $D=A/B$; κ is the apparent fluid viscosity; γ is the fluid's unit weight; τ_o is the initial shear strength of the fluid; and $b = 1/m$ where m is the exponent of a power function that represents the fluid's stress (τ_s)-rate of strain (dv/dy) relation, i.e., $\tau_s = \tau_o + \kappa(dv/dy)^m$ in which v and y are the flow velocity and depth, respectively.

There may be various locations (internal boundaries) along the main-stem river and/or tributaries where the flow is rapidly varied in space and Eqs. (1-2) are not applicable, e.g. dams, bridges/road-embankments, waterfalls, short steep rapids, weirs, etc. The following equations are used in lieu of Eqs. (1-2) at internal boundaries:

$$Q_i - Q_{i+1} = 0 \quad \ldots\ldots\ldots(4)$$

$$Q_i = f(h_i, h_{i+1}, \text{properties of control structure}) \quad \ldots\ldots\ldots(5)$$

in which the subscripts i and i+1 represent sequential cross sections located just upstream and just downstream of the structure, respectively. If the structure is a bridge, then Eq. (5) assumes the following form:

$$Q = \sqrt{2g}\,C_b A_b\,(h_i - h_{i+1} + v^2/2g - \Delta h_f)^{1/2} + C_e L_e K_e (h_i - h_e)^{3/2} \quad \ldots\ldots\ldots(6)$$

in which C_b is the coefficient of flow through the bridge, A_b is the wetted cross-sectional area of the bridge opening, $v = Q/A$, Δh_f is the head loss through the bridge, C_e is the coefficient of discharge for flow over the embankment, L_e is the length of the road embankment, h_e is the elevation of the embankment crest, and K_e is a broad-crested weir submergence correction, i.e., $K_e = 1-23.8[(h_{i+1} - h_e)/(h_i - h_e) - 0.67]^3$. If the flow structure is a dam, then Eq. (5) assumes the following form:

$$Q=K_s C_s L_s (h_i-h_s)^{3/2} + \sqrt{2g}\, C_g A_g (h_i-h_g)^{1/2} + K_d C_d L_d (h_i-h_d)^{3/2} + Q_t + Q_{br} = 0 \quad \ldots\ldots\ldots (7)$$

in which K_s, C_s, L_s, h_s are the uncontrolled spillway's submergence correction factor, coefficient of discharge, length of spillway, and crest elevation, respectively; K_d, C_d, L_d, h_d are similar properties of the crest of the dam; C_g, A_g, h_g are the coefficient of discharge, area, and height of opening of a fixed or time-dependent moveable gate spillway; Q_t is a constant or time-dependent turbine discharge; and Q_{br} is the flow through a time-dependent breach of the dam (Fread, 1977) given by the following:

$$Q_{br} = C_v K_b [3.1\, b_i (h_i - h_b)^{3/2} + 2.45\, Z\, (h - h_b)^{5/2}] \quad \ldots\ldots\ldots (8)$$

in which b_i is the known time-dependent bottom width of the breach, h_i is the known time-dependent bottom elevation of the breach, Z is the side slope of the breach (1: vertical to Z: horizontal), C_v is a velocity of approach correction factor, and K_b is a broad-crested weir submergence correction factor similar to K_e in Eq. (6). If the structure is a natural rapids or waterfall, then a simple critical flow equation can be used for Eq. (5). Also, empirical rating curves of Q versus h may be used in lieu of Eq. (5) or in place of any or all of the first three terms in Eq. (7).

The flow structure may be a navigational dam with an associated lock where minimal navigational depths are maintained upstream of the dam by a dam tender who operates adjustable gates which control the river flow. In this case, Eq. (5) takes the following form:

$$h_i = h_t \quad \ldots\ldots\ldots (9)$$

where h_t is the target pool elevation which the dam tender attempts to maintain via operation of the gates. The target pool elevation may be a constant value, or it may be specified as a function of time and read-in as a time series. When the simulated tailwater elevation exceeds a specified tailwater elevation, the flow is computed via Eqs. (1-2).

External boundary equations at the upstream or downstream extremities of the waterway must be specified to obtain solutions to the Saint-Venant equations. In fact, in many applications, the unsteady disturbance is introduced to the waterway at one or more of the external boundaries via a specified time series of discharge (a discharge hydrograph) or water elevation as in the case of a lake level or estuarial tidal fluctuation. If the water surface of the most upstream reservoir is assumed to remain level as it varies with time due to the inflows and spillway/breach outflows, then the following upstream boundary equation is used:

$$Q_1 = QI(t) - 0.5\, \bar{S}_a\, 43560.\, \Delta h/\Delta t \quad \ldots\ldots\ldots (10)$$

in which Q_1 is the discharge at the upstream most section (the upstream face of the dam), QI(t) is the specified inflow to the reservoir, $\bar{S}_a$ is the average surface area (acre-ft) of the reservoir during the Δt time interval, and Δh is the change in reservoir elevation during the time step. Eq. (10) represents a level-pool routing algorithm in the form of an upstream boundary condition. The use of Eq. (10) requires that a table of reservoir surface area versus elevation be specified. At the downstream extremity or N^{th} cross section, the boundary equation could be Eq. (7), an empirical rating of h and Q, or a

channel control, loop-rating based on the Manning equation in which S (the dynamic energy slope) is approximated by:

$$S = (h_{N-1} - h_N)/\Delta x - (Q^{t+\Delta t} - Q)/(gA\ \Delta t) - [(Q^2/A)_N - (Q^2/A)_{N-1}]/(gA\ \Delta x) \quad (11)$$

in which Δx represents the reach length between the last two cross sections at the downstream extremity of the waterway.

Solution Technique

The Saint-Venant Eqs. (1-2) cannot be solved directly; however they can be solved by finite-difference approximations. The FLDWAV model utilizes a weighted four-point nonlinear implicit finite-difference solution technique as described by (Fread, 1985). Substitution of appropriate simple algebraic approximations for the derivative and non-derivative terms in Eqs. (1-2) result in two nonlinear algebraic equations for each Δx reach between specified cross sections which, when combined with the external boundary equations and any necessary internal boundary equations, may be solved by an iterative quadratic solution technique (Newton-Raphson) along with an efficient, compact, quad-diagonal Gaussian elemination matrix solution technique. Initial conditions are also required at $t = 0$ to start the solution technique. These are automatically obtained within FLDWAV via a steady flow back-water solution or they may be specified as data input for unsteady flows occurring at $t = 0$.

A river system consisting of a main-stem river and one or more principal tributaries is efficiently solved using an iterative relaxation method (Fread, 1973) in which the flow at the confluence of the main-stem and tributary is treated as the lateral inflow/outflow term (q) in Eqs. (1-2). This method solves during a time step the unsteady flow equations first for the main stem, and then for each tributary of the river system. The tributary flow at the confluence with the main-stem river is treated as a lateral flow q which is first estimated when solving the equations for the main stem. The tributary flow depends on its upstream boundary condition, lateral inflows along its reach,and the water surface elevation at the confluence (downstream boundary for the tributary) which is obtained during the simulation of the main stem. Due to the interdependence of the flows in the main stem and its tributaries, the following iterative or relaxation algorithm is used:

$$q^* = \alpha\, q + (1-\alpha)\, q^{**} \quad (12)$$

in which α is a weighting factor ($0 < \alpha \leq 1$), q is the computed tributary flow at the confluence, q^{**} is the previous estimate of q, and q^* is the new estimate of q. Convergence is attained when q^* is sufficiently close to q^{**}. Usually, one or two iterations is sufficient; however, the α weighting factor has an important influence of the algorithm's efficiency. Optimal values of α can reduce the irerations by as much as 1/2. A priori selection of α is difficult since α varies with each river system. Good first approximations for α are in the range, $0.6 \leq \alpha \leq 0.8$ and the optimal α value may be obtained by trial-and-error. FLDWAV can accommodate any number of 1st order tributaries. Systems with 2nd order tributaries can sometimes be accommodated by reordering the system, i.e., selecting another branch of the system as the main stem.

If the river consists of bifurcations such as islands and/or complex dendritic systems with tributaries connected to tributaries, etc., a network solution technique is used (Fread, 1985), wherein three internal boundary equations conserve mass and momentum at each confluence, i.e.,

$$Q_i^{j+1} + Q_{i'}^{j+1} - Q_{i'+1}^{j+1} - \Delta s/\Delta t^j = 0 \quad \text{.....(13)}$$

$$2g\,(h_i^{j+1} - h_{i'+1}^{j+1}) + (Q^2/A^2)_i^{j+1} - T\,(Q^2/A^2)_{i'+1}^{j+1} = 0 \quad \text{.....(14)}$$

$$2g\,(h_{i'}^{j+1} - h_{i'+1}^{j+1}) + (Q^2/A^2)_{i'}^{j+1} - T\,(Q^2/A^2)_{i'+1}^{j+1} = 0 \quad \text{.....(15)}$$

where:

$$\frac{\Delta s}{\Delta t} = \Delta x_i/(6\Delta t^j)\,\tilde{B}\,(h_i^{j+1} + h_{i'}^{j+1} + h_{i'+1}^{j+1} - h_i^j - h_{i'}^j - h_{i'+1}^j) \quad \text{.....(16)}$$

$$i' = i + m + 1 \quad \text{.....(17)}$$

$$\tilde{B} = B_i^j + B_{i'+1}^j + B_{i'}^j \cos\omega_t \quad \text{.....(18)}$$

$$T = 1 + C_m + C_f \quad \text{.....(19)}$$

$$C_m = (0.1 + 0.83\,Q_{i'}^j/Q_{i'+1}^j)\,(\omega_t/90)^\mu \quad \text{.....(20)}$$

$$C_f = 2g\,\Delta x_i\,\bar{n}^2/[2.21\,(\bar{D}^{-4/3})^j] \quad \text{.....(21)}$$

in which $\bar{D}$ is the average depth in the junction, $\bar{n}$ is the Manning n for the junction, ω_t is the acute angle between the upstream reach and the branch, μ is an exponent assumed to be unity, and m is the total number of Δx reaches located upstream (downstream) along the branching channel. The parameters C_f and C_m are related to friction effects and to the head loss due to mixing as reported by Lin and Soong (1979), respectively. The superscript (j) and the subscript (i) represent respectively the time line and cross section location in the x-t computational plane.

This method of simulating a network of channels maintains a nonlinear formulation of the entire system, thus retaining the Newton-Raphson iterative equation solver, and yet performs the computations quite efficiently. The matrix is 2N x 2N where N is the total number of cross sections. Since it is not possible to maintain a diagonally banded matrix for the coefficients introduced via Eqs. (13-15) in the composition of the coefficient matrix, the number of off-diagonal elements and their consequences can be minimized by using a special Gauss elimination matrix solution technique that operates only on non-zero off-diagonal elements. The number of operations (addition, subtraction, multiplication, division) required to solve the matrix is approximately (102 + 46J)N, where J is the total number of junctions. This is compared to (95N-48) operations for the relaxation algorithm, (38N-19) for a single channel and $(5N^3+8N^2+5N)$ for a standard Gauss elimination method. For example, if N = 100 and J = 5, the network algorithm requires 33,200 operations, while the relaxation method requires 9452 operations (but it is not applicable to networks other than first order dendritic), and the standard Gauss method requires 5,080,500 operations.

Subcritical/Supercritical Algorithm

This optional algorithm (Fread, 1985) automatically subdivides the total routing reach into sub-reaches in which only subcritical (Sub) or supercritical (Sup) flow occurs. The transition locations where the flow changes from Sub to Sup or vice versa are treated as external boundary conditions. This avoids the application of the Saint-Venant equations to the critical flow transitions. At each time step, the solution commences with the most upstream sub-reach and proceeds sub-reach by sub-reach in the downstream direction. The upstream boundary (UB) and downstream boundary (DB) are automatically selected as follows: (1) when the most upstream sub-reach is Sub, the UB is the specified discharge hydrograph and the DB is the critical flow equation since the next downstream sub-reach is Sup; (2) when the most upstream sub-reach is Sup, the UB is the specified hydrograph and a loop-rating quite similar to that previously described as an external boundary condition, and no DB is required since flow disturbances created downstream of the Sup reach cannot propagate upstream into this sub-reach; (3) when an inner sub-reach is Sup, its two UB conditions are the discharge just computed at the DB of the adjacent upstream sub-reach and the computed critical water surface elevation at the same DB; (4) when an inner sub-reach is Sub, its UB is the discharge just computed at the most downstream section of the adjacent upstream Sup sub-reach and the DB is the critical flow equation. Hydraulic jumps are allowed to move either upstream or downstream prior to advancing to another computational time step; this is accomplished by comparing computed sequent elevations (h_s) with computed backwater elevations (h) at each section in the vicinity of the hydraulic jump. The jump is moved section by section upstream until $h_s > h$ or moved downstream until $h > h_s$. The Froude number $\left(Fr = Q/(A\sqrt{gD})\right)$ is used to determine if the flow at a particular section is Sub or Sup, i.e., if $Fr<1$ the flow is Sub and if $Fr \geq 1$ the flow is Sup. The Sub/Sup algorithm increases the computational requirements by approximately 20 percent.

Levee Overtopping

Flows which overtop levees located along either or both sides of a main-stem river and/or its principal tributaries may be simulated within FLDWAV. The overtopping flow is considered lateral outflow (-q) in Eqs. (1-2), and is computed as broad-crested weir flow. Three options exist for simulating the interaction of the overtopping flow with the receiving floodplain area. The first option simply ignores the presence of the floodplain and is described later in the subsection on lateral flows. The second option treats the receiving floodplain as a storage or ponding area having a user-specified storage-elevation relationship. The floodplain water surface elevations are computed via the simple storage (level-pool) routing equation, i.e. inflow-outflow = temporal change in storage. The overtopping broad-crested weir flow is corrected for submergence effects if the floodplain water elevation exceeds sufficiently the levee crest elevation. In fact, the overtopping flow may reverse its direction if the floodplain elevation exceeds the river surface water elevation. The overtopping flow is computed according to the following:

$$q = -C\, K_s\, (h - h_c)^{3/2} \qquad (22)$$

where:

$K_s = 1.0$ if $h_r \leq 0.67$ .....(23)

$K_s = 1.0 - 27.8\ (Y - 0.67)^3$ if $h_r > 0.67$ .....(24)

$h_r = (h_{fp} - h_c)/(h - n_c)$ .....(25)

in which C = discharge coefficient, K_s = submergence correction factor, h_c = levee crest elevation, h = water elevation of river, and h_{fp} = water elevation of floodplain. In the third option the floodplain is treated as a tributary of the river and the Saint-Venant equations are used to determine its flow and water surface elevations; the overtopping levee flow is considered as lateral inflow (q) in Eqs. (1-2). In each option the levee may also crevasse (breach) along a user-specified portion of its length.

If the receiving floodplain area is divided into separate compartments by additional levees or road-embankments located perpendicular to the river and its levees, the flow transfer from a compartment to an adjacent upstream or downstream compartment is simulated via broad-crested weir flow with submergence correction; flow reversals (outflows) can occur when dictated by the water surface elevations within adjacent compartments, which are computed by the storage routing equation as in the second option. The compartment elevation (h_{fp}) is obtained iteratively via a table look-up algorithm applied to the specified table of volume-elevation values. The outflow from a floodplain compartment may also include that from one or more pumps associated with each floodplain compartment. Each pump has a specified discharge-head relation given in tabular form along with start-up and shut-off operation instructions as delineated by specified water surface elevations. The pumps discharge to the river.

Automatic Calibration

An option within FLDWAV allows the automatic determination of the Manning n such that the difference between computed water surface elevations (stage hydrographs) and observed hydrographs is minimized. The Manning n can vary with either flow or water elevation and with sub-reaches separated by water level recorders. The algorithm (Fread and Smith, 1978) for efficiently accomplishing this is applicable to a single multiple-reach river or a main-stem river and its principal tributaries. The algorithm is based on a scheme of decomposing complex river systems of dendritic configuration. Optimum Manning n values are sequentially determined for each reach bounded by gaging stations, commencing with the most upstream reach, and progressing reach by reach in the downstream direction. Tributaries are calibrated before the main stem river and their flows are added to the main stem as lateral inflows. Discharge is input at the upstream boundary of each river, while observed stages at the downstream gaging station of each reach is used as the downstream boundary condition. Computed stages at the upstream boundary are tested against observed stages at that point. Statistics of bias (Φ_j) and root-mean-square (RMS) error are computed for several (j) ranges of discharge or stage so that the Manning n can be calibrated as a function of discharge or stage. For each range of discharge, an improved estimate of the optimum Manning n (n_j^{k+1}) is obtained via a modified Newton-Raphson iterative algorithm, i.e.,

$$n_j^{k+1} = n_j^k - \frac{\Phi_j^k (n_j^k - n_j^{k-1})}{\Phi_j^k - \Phi_j^{k-1}} \qquad k \geq 2;\ j = 1,2,\ldots J \quad \ldots\ldots\ldots\ldots\ldots\ldots (26)$$

in which the k superscript denotes the number of iterations and Φ_j is the bias for the j^{th} range. Eq. (26) can be applied only for the second and successive iterations; therefore, the first iteration is made using the following algorithm:

$$n_j^{k+1} = n_j^k \ (1.0 - 0.01 \ \Phi_j^k / |\Phi_j^k|) \qquad k = 1;\ j = 1,2,\ldots J \quad \ldots\ldots\ldots\ldots\ldots\ldots (27)$$

in which a small percentage change in n is made in the correct direction as determined by the term $(-\Phi_j^k/|\Phi_j^k|)$. The convergence properties of Eq. (26) are quadratic with convergence usually obtained within three to five iterations. Improved n values obtained via Eq. (26) are used and the cycle repeated until a minimum RMS error for the reach is found. Then, the discharges computed at the downstream boundary using the optimum Manning n are stored internally and then input as the upstream boundary condition for the next downstream reach.

FLDWAV also provides an option to conveniently utilize a methodology (Fread and Lewis, 1988) for determining optimal n values which may for some applications eliminate the need for time-consuming preparation of detailed cross-sectional data. Approximate cross sections represented by separate 2-parameter power functions for the channel and the floodplain are used. Optimized n values can be constrained to fall within user-specified min-max ranges. Also, specific cross-sectional properties at key sections (bridges, natural constrictions, etc.) can be utilized wherever considered appropriate.

Dam Breach Parameters

The breach is the opening formed in the dam as it fails. The actual failure mechanics are not well understood for either earthen or concrete dams. In FLDWAV the breach is assumed to develop over a finite interval of time (τ) and will have a final size determined by a terminal bottom width parameter (b) and various shapes depending on another parameter (Z), the side slope of the breach which depends on the angle of repose of the dam's materials. This parametric representation of the breach follows Fread and Harbaugh (1973) and is utilized in FLDWAV for reasons of simplicity, generality, wide applicability, and the uncertainty in the actual failure mechanism. The model assumes the breach bottom width starts at a point and enlarges at a linear or nonlinear rate over the failure time (τ) until the terminal bottom width (b) is attained and the breach bottom has eroded to the elevation h_{bm}. If τ is less than one minute, the width of the breach bottom starts at a value of b rather than zero. This represents more of a collapse failure than an erosion failure. The bottom elevation of the breach is simulated as a function of time (τ) according to the following:

$$h_b = h_d - (h_d - h_{bm})\left(\frac{t_b}{\tau}\right)^{\rho} \qquad \text{if} \quad 0 < t_b \leq \tau \quad \ldots\ldots\ldots\ldots\ldots\ldots (28)$$

in which h_{bm} is the final elevation of the breach bottom which is usually, but not necessarily, the bottom of the reservoir or outlet channel bottom, t_b is the time since beginning of breach formation, and ρ is the parameter specifing the degree of nonlinearity, e.g., ρ=1 is a linear formation rate, while ρ=2 is a nonlinear quadratic rate; the range for ρ is $1 \leq \rho \leq 4$; however, the linear

rate is usually assumed. The instantaneous bottom width (b_i) of the breach is given by the following:

$$b_i = b(t_b/\tau)^{\rho} \qquad \text{if} \quad 0 < t_b \leq \tau \qquad \text{.....(29)}$$

During the simulation of a dam failure, the actual breach formation commences when the reservoir water surface elevation (h) exceeds a specified value, h_f. This feature permits the simulation of an overtopping of a dam in which the breach does not form until a sufficient amount of water is flowing over the crest of the dam. A piping failure may also be simulated by specifing the initial centerline elevation of the pipe.

Concrete gravity dams tend to have a partial breach as one or more monolith sections formed during the construction of the dam are forced apart and over-turned by the escaping water. The time for breach formation is in the range of a few minutes. Concrete arch dams tend to fail completely and are assumed to require only a few minutes for the breach formation. The shape parameter (Z) is usually assumed zero for concrete dams.

Earthen dams which exceedingly outnumber all other types of dams do not tend to completely fail, nor do they fail instantaneously. The fully formed breach in earthen dams tends to have an average width ($\bar{b}$) in the range ($h \leq \bar{b} \leq 5h_d$) where h_d is the height of the dam. The middle portion of this range for $\bar{b}$ is supported by the summary report of Johnson and Illes (1976) and the upper range by the report of Singh and Snorrason (1982). Breach widths for earthen dams are therefore usually much less than the total length of the dam as measured across the valley. Also, the breach requires a finite interval of time (τ) for its formation through erosion of the dam materials by the escaping water. Total time of failure (for overtopping) may be in the range of a few minutes to usually less than an hour, depending on the height of the dam, the type of materials used in construction, the extent of compaction of the materials, and the magnitude and duration of the overtopping flow of the escaping water. The time of failure as used in DAMBRK is the duration of time between the first breaching of the upstream face of the dam until the breach is fully formed. For overtopping failures the beginning of breach formation is after the downstream face of the dam has eroded away and the resulting crevasse has progressed back across the width of the dam crest to reach the upstream face. Piping failures occur when initial breach formation takes place at some point below the top of the dam due to erosion of an internal channel through the dam by the escaping water. Times of failure are usually considerably longer for piping than overtopping failures since the upstream face is slowly being eroded in the very early phase of the piping development. As the erosion proceeds, a larger and larger opening is formed; this is eventually hastened by caving-in of the top portion of the dam. Poorly constructed coal-waste slag piles (dams) which impound water tend to fail within a few minutes, and have average breach widths in the upper range of the earthen dams mentioned above.

Recently some statistically derived predictors for $\bar{b}$ and τ have been presented in the literature, i.e., MacDonald and Langridge-Monopolis (1984) and Froelich (1987). From Froelich's work in which he used the properties of 43 breaches of dams ranging in height from 15 to 285 ft with all but 6 between 15 and 100 ft, the following predictive equations can be obtained:

$$\bar{b} = 9.5\, k_o\, (V_r\, h_d)^{0.25} \quad \text{.....(30)}$$

$$\tau = 0.8\, (V_r / h_d^2)^{0.50} \quad \text{.....(31)}$$

in which $\bar{b}$ is average breach width (ft), τ is time of failure (hrs), k_o = 1.0 for piping and 1.4 for overtopping, V_r is volume (acre-ft) and h_d is the height (ft) of water over the breach bottom which is usually about the height of the dam. Standard error of estimate for $\bar{b}$ was ±94 ft which is an average error of ±54% of $\bar{b}$, and the standard error of estimate for τ was ±0.9 hrs which is an average error of ±70% of τ.

Another means of determining the breach properties is the use of physically based breach erosion models. Recently the author (Fread, 1984, 1987) developed such a model (BREACH) which is described later herein.

Landslide-Generated Waves

Reservoirs are sometimes subject to landslides which rush into the reservoir, displacing a portion of the reservoir contents and, thereby, creating a very steep water wave which travels up and down the length of the reservoir (Davidson and McCartney, 1975). This wave may have sufficient amplitude to overtop the dam and precipitate a failure of the dam, or the wave by itself may be large enough to cause catastrophic flooding downstream of the dam without resulting in the failure of the dam as in the case of a concrete dam in Vaiont, Italy in 1963.

The capability to generate waves produced by landslides is provided within FLDWAV. The volume of the landslide mass, its porosity, and the time interval over which the landslide occurs are specified as input to the model. In the model, the landslide mass is deposited during very small computational time steps within the reservoir in layers commencing at the center of the reservoir and extending toward the side of the landslide, and simultaneously the original dimensions of the reservoir are reduced. The time rate of reduction in the reservoir cross-sectional area (Koutitas, 1977) creates the wave during the solution of the unsteady flow Eqs. (1-2), which are applied to the reservoir cross sections.

Wave runup is <u>not</u> considered in the model. For near vertical faces of concrete dams the runup may be neglected; however, for earthen dams the usual angle of the earthfill on the reservoir side will result in a surge that advances up the face of the dam to a height approximately equal to 2.5 times the height of the landslide-generated wave (Morris and Wiggert, 1972).

Lateral Flows

Unsteady flows associated with tributaries along the routing reach can be added to the unsteady flow resulting from the dam failure. This is accomplished via the term q in Eqs. (1-2). The tributary flow is distributed along a single Δx reach. Within the FLDWAV model, Q(t) is divided by Δx to obtain q(t). Backwater effects of the routed flow on the tributary flow are ignored, and the lateral tributary flow is assumed to enter perpendicular to

the routed flow. Outflows are assigned negative values. Outflows which occur as broad-crested weir flow over a levee or natural crest may be simulated within the FLDWAV model, i.e.,

$$q = -C_w (\bar{h} - h_w)^{1.5} \quad \text{.....(32)}$$

in which C_w is the discharge coefficient for broad-crested weir flow ($2.6 \leq C_w \leq 3.2$), $\bar{h}$ is the average of the computed water elevations at sections i and i+1 bounding the Δx reach in which the weir outflow occurs, and h_w is the average crest elevation of the weir along the Δx reach. The crest elevation, discharge coefficient, and location along the river/valley must be specified by the user.

Cross Section and Flow Resistance Parameters

In FLDWAV, active cross sections which convey flow may be of irregular as well as regular geometrical shape. Each cross-section is read-in as tabular values of channel width and elevation, which together constitute a piece-wise linear relationship. Experience has shown that in most instances the cross-section may be sufficiently described with eight or less sets of widths and associated elevations. A low-flow cross-sectional area which can be zero is used to describe the cross section below the minimum elevation read-in. From this input, the cross-sectional area associated with each of the widths is initially computed within the model. During the solution of the unsteady flow equations, any areas or widths associated with a particular water surface elevation are linearly interpolated from the piece-wise linear relationships.

Dead storage areas wherein the flow velocity in the x-direction is considered negligible relative to the velocity in the active area of the cross section is a feature of FLDWAV. Such dead or off-channel storage areas can be used to effectively account for embayments, ravines, or tributaries which connect to the flow channel but do not convey flow and serve only to store the flow. The dead storage cross-sectional properties are described similarly to those of the active cross sections.

The Manning n is used to describe the resistance to flow caused by bed forms, bank vegetation and obstructions, bend effects, and small scale eddy losses. The Manning n can vary considerably with flow elevation, i.e., the n value can be considerably larger for flow inundating the floodplain than flow confined within the channel bank. It can be larger for lesser floodplain depths than for greater flow depths; however, within the channel banks, the n value may decrease with increasing flow depth. The Manning n is defined for each channel reach bounded by gaging stations and is specified as a function of either stage or discharge via a piece-wise linear relation specified as input in tabular form. Linear interpolation is used to obtain n for values of h or Q intermediate to the tabular values. Simulation results are often sensitive to the Manning n. Although in the absence of necessary data (observed stages and discharges), n can be estimated, best results are obtained when n is adjusted to reproduce historical observations of stage and discharge. Such an adjustment process is known as calibration which may be either trial-and-error or an automatic technique described previously.

Program Structure

The FLDWAV model is coded in FORTRAN with over 80 subroutines which provide the desired modularity for future expansions to enable the simulation of other hydraulic phenomena. Arrays are coded with a variable dimensioning technique which utilizes a single, large array as the only array of fixed size. At each execution of the model, the large array is automatically partitioned into individual variable arrays required for a particular hydraulic application. The size of each array is automatically determined by user-specified data which describes the hydraulic application. This program structure allows maximum utilization of storage space since arrays not used during a particular simulation require no storage space.

The FLDWAV model's input/output is in either English or metric units. The input is either batch or interactive. The output form is numerical tabular and/or graphical.

Testing and Verification

The FLDWAV model has been tested and verified on several rivers throughout the United States. The applications include the following: (1) a dendritic river system consisting of 393 miles(629 km) of the Mississippi-Ohio-Cumberland-Tennessee rivers schematically shown in Fig. 1 (an example of this application is shown in Fig. 2, the computed vs. simulated stages for Cairo at the junction of the Mississippi and Ohio rivers); (2) a 292 mile(469 km) reach of the lower Mississippi which was calibrated for a 1969 flood using records of six gaging stations located throughout the reach; the average route-mean-square (RMS) error between the computed and observed water levels was 0.25 ft(0.08 m) and for the years 1959-71 using the 1969 calibration was 0.47 ft(0.15 m) with a maximum average RMS value during test period of 0.91 ft(0.28 m); (3) a 130 mile(209 km) reach of the tidal affected lower Columbia river including a 25 mile(40 km) tributary reach of the Willamette; the average RMS error for seven gaging stations was 0.21 ft(0.06 m) for stage hydrographs with a diurnal tidal fluctuation of as much as seven feet(2.13 m); (4) a dendritic river system consisting of 463 miles(744 km) of the Upper Mississippi-Illinois-Missouri rivers and 9 locks and dams; the average RMS error for 18 water level recording stations was 0.38 ft(0.12 m); (5) a 60 mile(96 km) reach of the Teton-Snake rivers located downstream of 262 ft(79.8 m) high Teton dam which failed in 1976 (Ray, et al., 1976) producing a peak discharge in excess of 2 million cfs(56,800 cms); variations between computed and observed high water marks averaged about 1.5 ft(0.47 m) and differences between computed and observed discharges were less than 5 percent as indicated on the peak discharge profile of Fig. 3; and (6) a 16 mile(26 km) reach of Buffalo Creek located downstream of 44 ft(13.4 m) high coal-waste dam which failed in 1972 (Davies, et al., 1975) producing a peak discharge of over 80,000 cfs(2270 cms); variations between computed and observed high water marks averaged about 1.8 ft(0.55 m) and peak discharges compared within an average of 9 percent variation with observed values as shown in Fig. 4.

DWOPER MODEL

The DWOPER model (Fread, 1978) is based on the following form of the Saint-Venant equations:

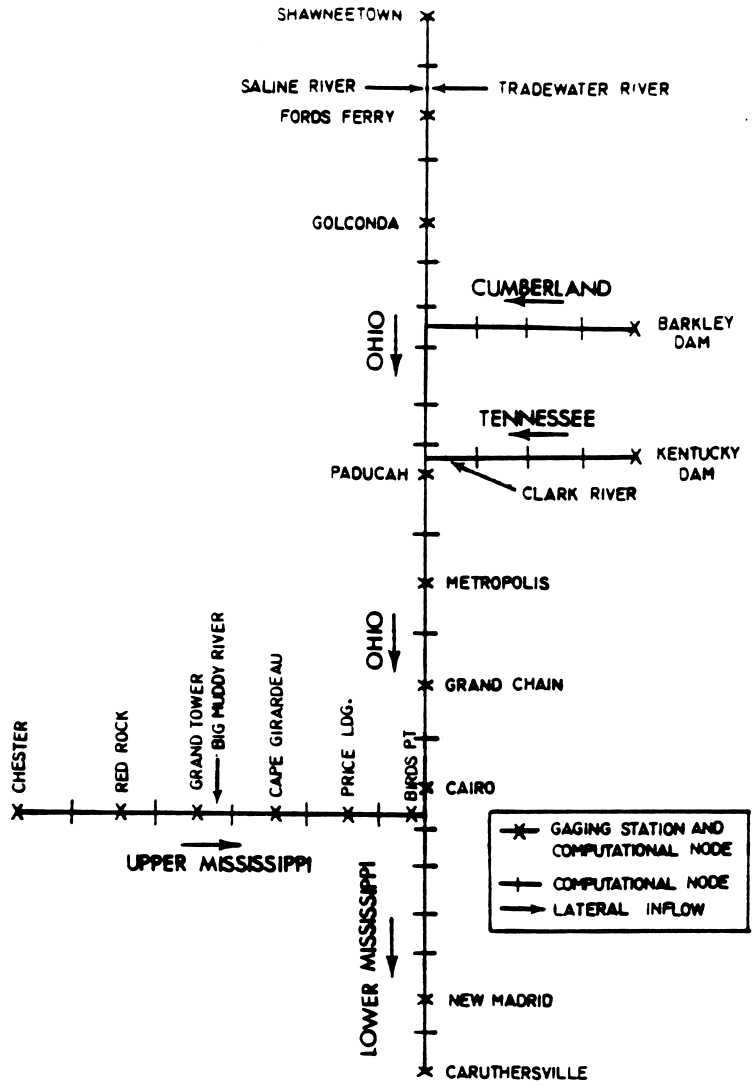

Fig. 1 Schematic of Mississippi-Ohio-Cumberland-Tennessee River System

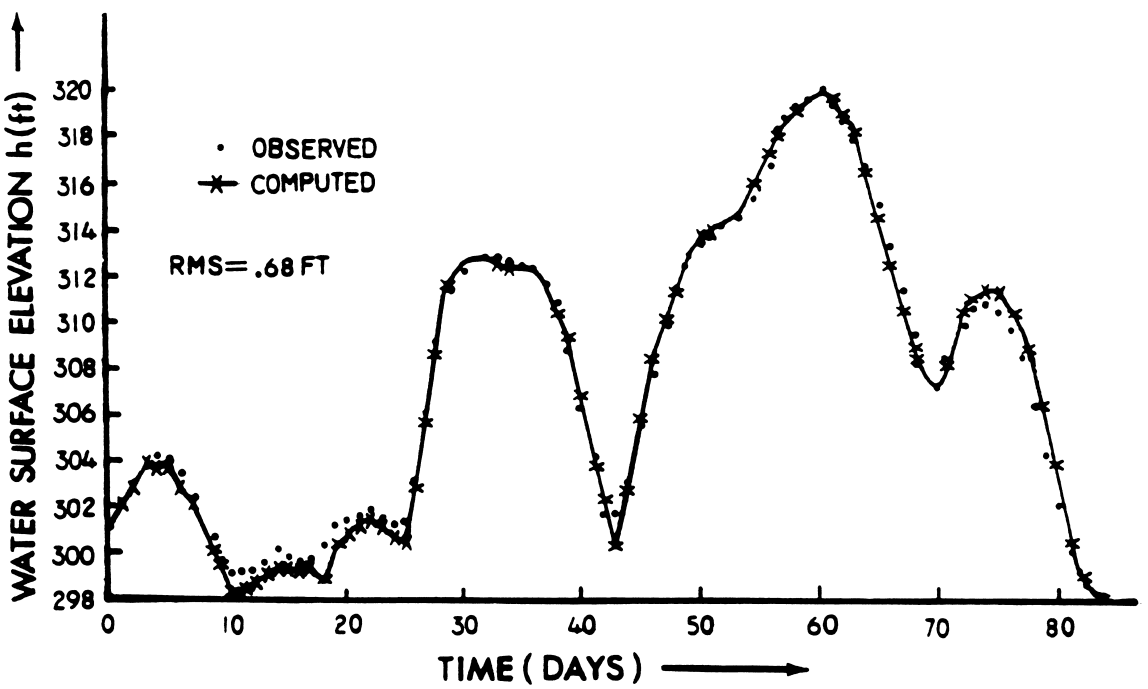

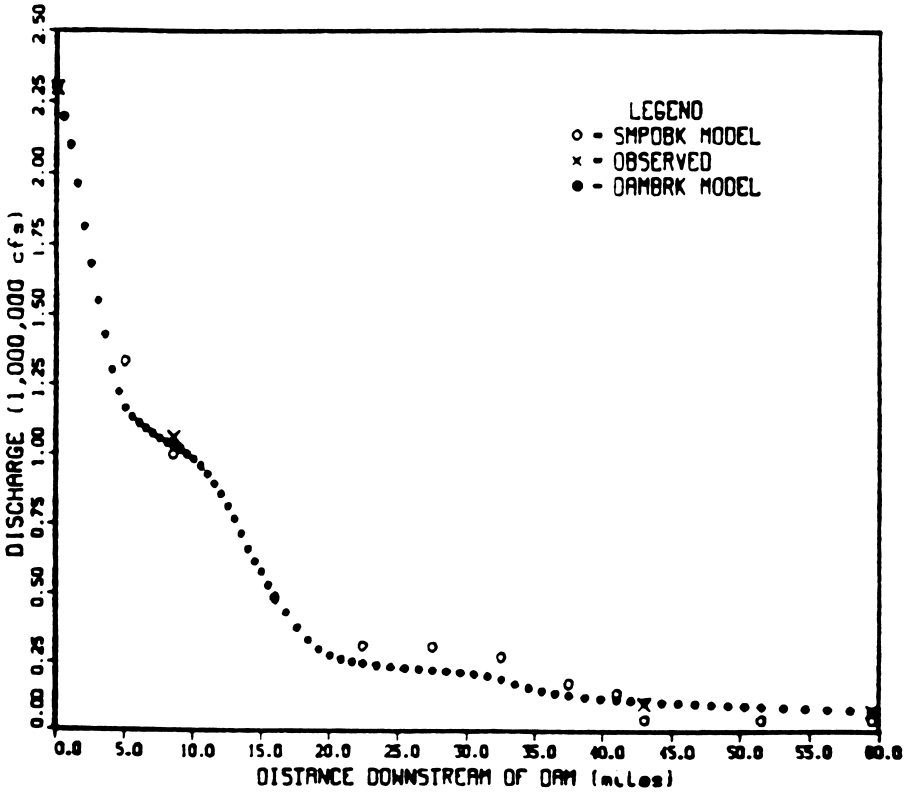

FIG. 3 PROFILE OF PEAK DISCHARGE DOWNSTREAM OF TETON.

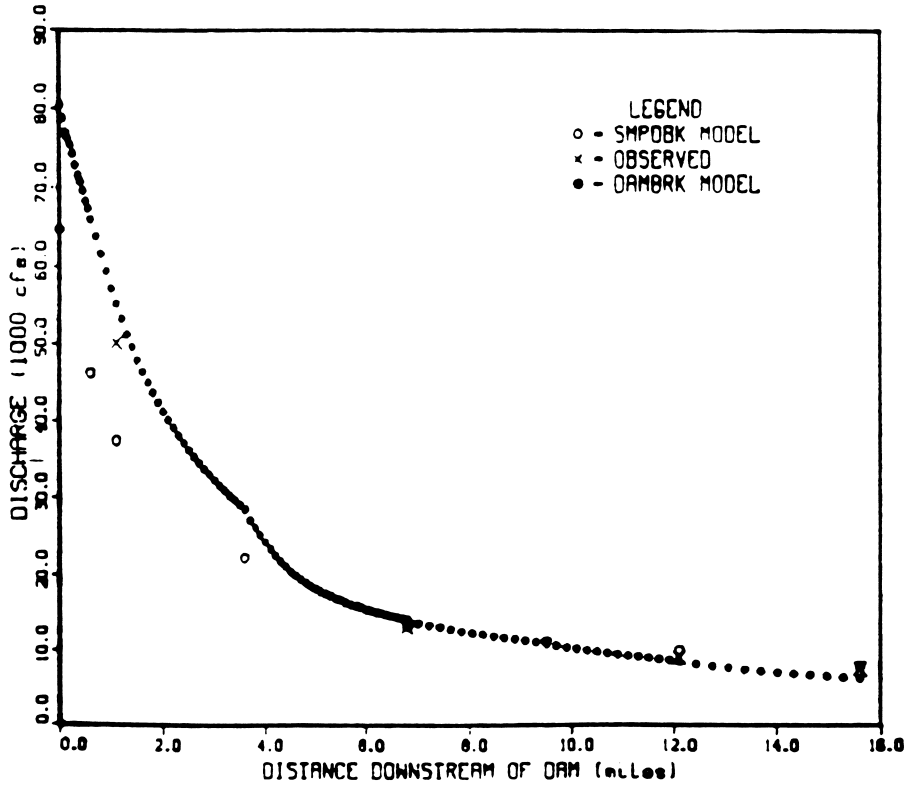

FIG. 4 PROFILE OF PEAK DISCHARGE DOWNSTREAM OF BUFFALO CREEK.

$$\partial Q/\partial x + \partial(A + A_o)/\partial t - q = 0 \quad \text{.....(33)}$$

$$\partial Q/\partial t + \partial(Q^2/A)/\partial x + gA(\partial h/\partial x + S_f + S_e) + L + W_f B = 0 \quad \text{.....(34)}$$

in which $S_f = n^2|Q|Q/(2.21\ A^2 R^{4/3})$ and all other terms are defined as in Eqs. (1-2), the governing equations of the FLDWAV model. The sinuosity coefficients (S_c and S_m) of Eqs. (1-2) are not included, and the friction slope (S_f) is defined in terms of the Manning n rather then the total conveyance. Also, the non-newtonian internal viscous dissipation slope (S_i) of Eqs. (1-2) for mud/debris flows is not included. Internal boundary conditions include bridges and dams; however, neither can be breached as in the FLDWAV model, and dams are represented by a rating curve (head vs. discharge) rather than Eq. 7.

The DWOPER model cannot accomodate supercritical flows or mixed subcritical/supercritical flows as can the FLDWAV model. Only the third option of levee overtopping in the FLDWAV model is available in the DWOPER model, i.e., the floodplain beyond the levee is treated as a tributary of the river contained by the levee. Although the DWOPER model provides an automatic calibration option as in the FLDWAV model, it does not have the option of 2-parameter power function representation of cross-sectional geometry as described by Fread and Lewis (1986). The DWOPER model does not have the metric input/output option. The DWOPER model does have the capability of modeling river systems with either the relaxation algorithm or the network algorithm, and DWOPER is programmed with variable dimensioned arrays.

DAMBRK MODEL

The DAMBRK model (Fread, 1977, 1984, 1988) is based on the following form of the Saint-Venant equations.

$$\partial Q/\partial x + \partial\, s_c(A + A_o)/\partial t - q = 0 \quad \text{.....(35)}$$

$$\partial(s_m Q)/\partial t + \partial(Q^2/A)/\partial x + gA(\partial h/\partial x + S_f + S_e + S_i) + L = 0 \quad \text{.....(36)}$$

in which all terms are defined as in Eqs. (1-2), the governing equations of the FLDWAV model. Eqs. (35-36) do not contain the wind factor (W_f) as in the FLDWAV model, and the lateral flow momentum term (L) does not include the effect of lateral inflow velocities that are not perpendicular to the receiving stream, i.e., $L = -qv_x$ is not an available option in the DAMBRK model.

Only a single river can be simulated with the DAMBRK model rather than a system of interconnected rivers which can be modeled by FLDWAV. The DAMBRK model uses Eqs. (4-8) for internal boundaries; thus, breached dams or bridge embankments can be simulated. DAMBRK can treat supercritical or mixed subcritical/supercritical flows as does FLDWAV. Only the first option of levee overtopping in FLDWAV is available in DAMBRK. The multiple floodplain compartments option is available in DAMBRK. Automatic calibration is not an option in DAMBRK. The metric input/output is available as in FLDWAV. DAMBRK is programmed with fixed arrays rather than variable dimensioned arrays as in FLDWAV.

SMPDBK MODEL

The SMPDBK model, as described in detail by Wetmore and Fread (1984) is a simple model for predicting the characteristics of the floodwave peak produced by a breached dam. It will, with minimal computational resources (hand-held calculators, microcomputers), determine the peak flow, depth, and time of occurrence at selected locations downstream of a breached dam. SMPDBK first computes the peak outflow at the dam, based on the reservoir size and the temporal and geometrical description of the breach. The computed floodwave and channel properties are used in conjunction with routing curves to determine how the peak flow will be diminished as it moves downstream. Based on this predicted floodwave reduction, the model computes the peak flows at specified downstream points. The model then computes the depth reached by the peak flow based on the channel geometry, slope, and roughness at these downstream points. The model also computes the time required for the peak to reach each forecast point and, if a flood depth is entered for the point, the time at which that depth is reached as well as when the floodwave recedes below that depth, thus providing a time frame for evacuation and fortification on which a preparedness plan may be based. The SMPDBK model neglects backwater effects created by downstream dams or bridge embankments, the presence of which can substantially reduce the model's accuracy. However, its speed and ease of use together with its small computational requirements make it an attractive tool for use in cases where limited time and resources preclude the use of the DAMBRK model. In such instances forecasters, planners, emergency managers, and consulting engineers responsible for predicting the potential effects of a dam failure may employ the model where backwater effects are not significant.

The SMPDBK model retains the critical deterministic components of the DAMBRK model while eliminating the need for extensive numerical computations. It accomplishes this by approximating the downstream channel/valley as a prism, concerning itself with only the peak flows, stages, and travel times, neglecting the effects of backwater from downstream bridges and dams, and utilizing dimensionless peak-flow routing graphs developed by using the DAMBRK model. The applicability of the SMPDBK model is enhanced with its user friendly interactive input and option for minimal data requirements. The peak flow at the dam may be computed with only four readily accessible data values and the downstream channel/valley may be defined with a single average cross section, although prediction accuracy greatly increases with the number of specified cross sections.

Breach Outflow

The model uses a single equation to determine the maximum breach outflow and the user is required to supply the values of four variables for this equation. These variables are: 1) the surface area (A_s, acres) of the reservoir; 2) the depth (H, ft) to which the breach cuts; this is usually the same value as the height of the dam plus the depth of overtopping flow; 3) the time (τ, hours) required for breach formation; and 4) the final width (B_r, ft) of the breach. These parameters are substituted into a broad-crested weir flow equation to yield the maximum breach outflow (Q_{bmax}) in cfs, i.e.,

$$Q_{bmax} = Q_o + 3.1\, B_r \left(\frac{C}{\tau + C/\sqrt{H}}\right)^3 \qquad (37)$$

where:

$$C = \frac{23.4\ A_S}{B_r} \quad \text{.....(38)}$$

and Q_o is the spillway flow and overtopping crest flow which is estimated to occur simultaneously with the peak breach outflow.

Once the maximum outflow at the dam has been computed, the depth of flow produced by this discharge may be determined based on the geometry of the channel immediately downstream of the dam, the Manning n (roughness coefficient) of the channel and the slope of the downstream channel. This depth is then compared to the depth of water in the reservoir to find whether it is necessary to include a submergence correction factor for tailwater effects on the breach outflow, i.e., to determine if the water downstream is restricting the free flow through the breach. This comparison and (if necessary) correction allows the model to provide the most accurate prediction of maximum breach outflow which properly accounts for the effects of tailwater depth downstream of the dam. The submergence correction factor (K_d) is similar to that in Eq. (8) and must be applied iteratively since the outflow produces the tailwater depth which determines the submergence factor which affects the outflow.

Peak Flow Routing

The peak discharge is routed to downstream points of interest through the channel/valley which is described by selected cross sections defined by tables of widths and associated elevations. The routing reach from the dam to the point of interest is approximated within SMPDBK as a prismatic channel by defining a single cross section (an average section that incorporates the geometric properties of all intervening sections via a distance weighting technique). This prismatic representation of the channel allows easy calculation of flow area and volume in the downstream channel which is required to accurately predict the amount of peak flow attenuation. The peak flow at the dam computed by Eq. (37) is routed downstream using the dimensionless routing curves (see Fig. 5). These curves were developed from numerous executions of the NWS DAMBRK model and they are grouped into families based on the Froude number associated with the floodwave peak,and have as their X-coordinate the ratio of the downstream distance (from the dam to a selected cross section) to a distance parameter (X_c). The Y-coordinate of the curves used in predicting peak downstream flows is the ratio of the peak flow at the selected cross section to the computed peak flow at the dam. The distinguishing characteristic of each member of a family is the ratio (V*) of the volume in the reservoir to the average flow volume in the downstream channel. Thus it may be seen that to predict the peak flow of the floodwave at a downstream point, the desired distinguishing characteristic of the curve family and member must be determined. this determination is based on the calculation of the Froude number (F_c) and the volume ration parameter (V*). To specify the distance in dimensionless form, the distance parameter (X_c) in ft is computed as follows:

$$X_c = 6\ VOL/[\bar{A}(1 + 4(0.5)^{m+1})] \quad \text{.....(39)}$$

in which VOL is the reservoir volume (acre-ft), m is a shape factor for the prismatic routing reach, and $\bar{A}$ is the average cross-section area in the routing reach at a depth corresponding to the height of the dam. The volume

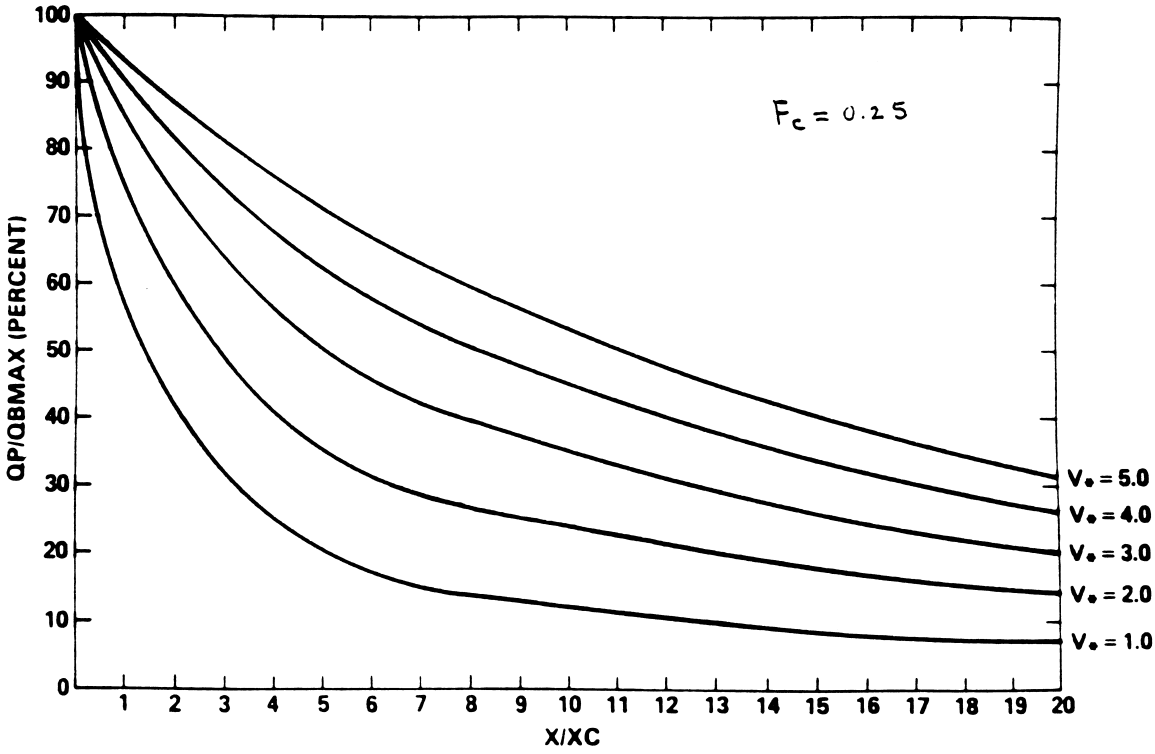

FIG. 5 ROUTING CURVES FOR SMPDBK MODEL FOR FROUDE NO = 0.25.

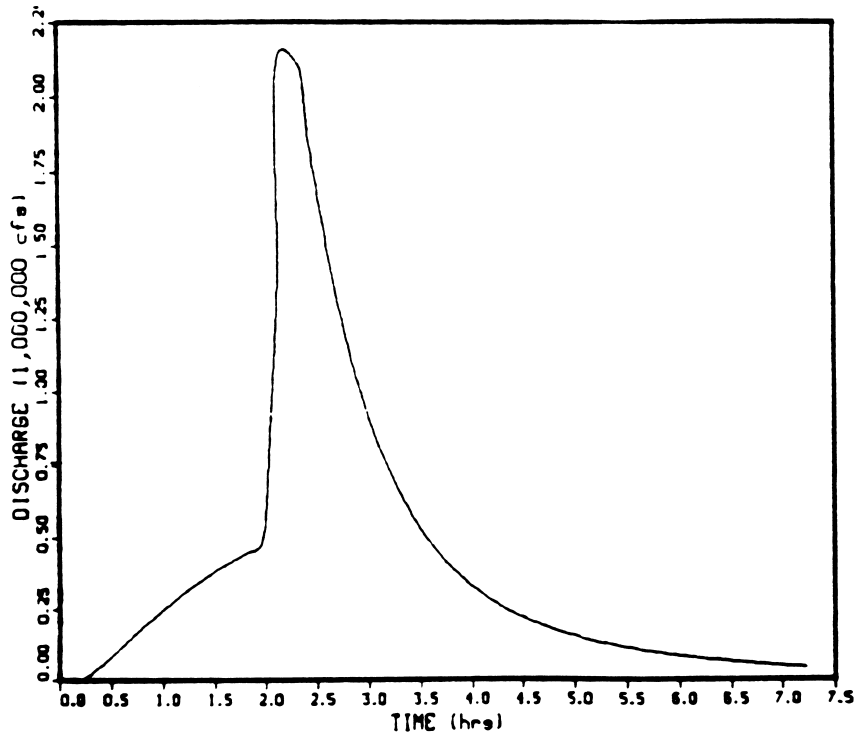

FIG 6. TETON OUTFLOW HYDROGRAPH PRODUCED BY BREACH MODEL.

parameter (V*) is simply $V^* = VOL/(\bar{A}_c X_c)$ in which $\bar{A}_c$ represents the average cross-sectional area in the routing reach at the average maximum depth produced by the routed flow. The Froude number (F_c) is simply $F_c = V_c/(gD_c)^{0.5}$ where V_c and D_c are the average velocity and hydraulic depth, respectively, within the routing reach. Using families of curves similar to Fig. 5, the routed peak discharge can be obtained. The corresponding peak depth is computed from the Manning equation using an iterative method since the wetted area and hydraulic radius are nonlinear functions of the unknown depth.

The time of occurrence of the peak flow at a selected cross section is determined by adding the time of failure to the peak travel time from the dam to that cross section. The travel time is computed using the kinematic wave velocity which is a known function of the average flow velocity throughout the routing reach. The times of first flooding and "de-flooding" of a particular elevation at the cross section may also be determined within SMPDBK. Further description of the computational procedure for determining these times, as well as the time of peak flow and dimensionless parameters, may be found in Wetmore and Fread (1984).

Testing and Verification

The SMPDKB model was compared with the DAMBRK model in several hypothetical applications where backwater effects were negligible. The average difference between the two models was 10-20 percent for predicted flows and travel times with depth differences of less than about 1 ft (0.3 m). Since the DAMBRK model is considered more accurate, the differences can be considered errors due to the simplifications of SMPDBK. The application of SMPDBK to the Teton dam breach is shown in Fig. 3, and its application to the Buffalo Creek "coal waste" dam is shown in Fig. 4. In each case, the peak discharge profile computed with the DAMBRK and FLDWAV models, and the observed peak flows are shown for comparison.

Additional testing of SMPDBK was conducted by Westphal and Thompson (1987) who concluded that SMPDBK produced peak discharges differing by an average of 13 percent from DAMBRK for six dams in the state of Missouri; the average difference between the two models for peak depths was about 2 ft (0.6 m).

BREACH MODEL

This model (Fread, 1984, 1987) predicts the outflow hydrograph from a breached dam and the breach size, shape, and time of formation of a breach in earthen/rockfill dams where the breach may be initiated by either piping or overtopping. The dam can be naturally formed by a landslide blockage of a river or man-made with either homogeneous fill or fill with a distinctive central core. The downstream face may be grass covered or bare. The model utilizes the principles of soil mechanics, hydraulics, and sediment transport to simulate the erosion and bank collapse processes which form the breach. Reservoir inflow, storage, and spillway characteristics, along with the geometrical and material properties of the dam (D_{50} size, cohesion, internal friction angle, porosity, and unit weight) are utilized to predict the outflow hydrograph. The essential model components are described as follows.

Reservoir Level

Conservation of mass is used to compute the reservoir water surface elevation (H) due to the influence of a specified reservoir inflow hydrograph (Q_i), spillway overflow (Q_{sp}) as determined from a spillway rating table, broad-crested weir flow (Q_o) over the crest of the dam, broad-crested weir flow (Q_b) through the breach, and the reservoir storage characteristics described by a surface area (S_a)-elevation table. Letting ΔH represent the change in reservoir level during a small time interval (Δt), the conservation of mass requires the following relationship:

$$\Delta H = \frac{0.0826\ \Delta t}{S_a} (\bar{Q}_i - \bar{Q}_b - \bar{Q}_{sp} - \bar{Q}_o) \quad \text{.....(40)}$$

in which the bar (-) denotes the average value during the Δt time interval. Thus, the reservoir elevation (H) at time (t) can easily be obtained since, $H = H' + \Delta H$, in which H' is the reservoir elevation at time $(t - \Delta t)$. If the breach is formed by piping, a short-tube, orifice flow equation is used instead of a broad-crested weir flow equation, i.e.,

$$Q_b = 3\ A_b(H - h_b)^{0.5} \quad \text{(broad-crested weir flow) .....(41)}$$

$$Q_b = A_b\ [2g(H-h_p)/(1 + fL/D)]^{0.5} \quad \text{(orifice flow) .....(42)}$$

in which A_b is the area of flow over the weir or orifice area, h_b is the elevation of the bottom of the breach at the upstream face of the dam, h_p is the specified center-line elevation of the pipe, f is the Darcy friction factor which is dependent of the D_{50} grain size, L is the length of the pipe, and D is the diameter or width of the pipe.

Breach Width

Initially the breach is considered rectangular with the width (B_0) based on the assumption of optimal channel hydraulic efficiency, $B_0 = B_r\ Y$, in which Y is the critical depth of flow at the entrance to the breach; i.e., $Y = 2/3(H-h_b)$. The factor B_r is set to 2 for overtopping and 1 for piping. The initial rectangular-shaped breach can change to a trapezoidal shape when the sides of the breach collapse due to the breach depth exceeding the limits of a free-standing cut in soil of specified properties of cohesion (C), internal friction angle (ϕ), unit weight (γ) and existing angle (θ') that the breach cut makes with the horizontal. The collapse occurs when the effective breach depth (d') exceeds the critical depth (d_c), i.e.,

$$d_c = 4C \cos\phi \sin\theta'/[\gamma - \gamma\cos(\theta' - \phi)] \quad \text{.....(43)}$$

The effective breach depth (d') is determined by reducing the actual breach depth (d) by Y/3 to account for the supporting influence of the water flowing through the breach. The θ' angle reduces to a new angle upon collapse which is simply $\theta = (\theta' + \phi)/2$. The model allows up to three collapses to occur.

Breach Erosion

Erosion is assumed to occur equally along the bottom and sides of the breach except when the sides of the breach collapse. Then, the breach bottom is assumed not to continue to erode downward until the volume of collapsed

material along the length of the breach is removed at the rate of sediment transport occurring along the breach at the instant before collapse. After this characteristically short pause, the breach bottom and sides continue to erode. Material above the wetted portion of the eroding breach sides is assumed to simultaneously collapse as the sides erode. Once the breach has eroded to the specified bottom of the dam, erosion continues to occur only along the sides of the breach and thus widening the breach. The rate at which the breach is eroded depends on the capacity of the flowing water to transport the eroded material. The Meyer-Peter and Muller sediment transport relation as modified by Smart (1984) for steep channels is used, i.e.,

$$Q_s = 3.64\ (D_{90}/D_{30})^{0.2}\ \frac{D^{2/3}}{n}\ P\ S^{1.1}\ (DS - 0.0054\ D_{50}\ \tau_c) \quad \text{.....(44)}$$

in which Q_s is the sediment transport rate, D_{90}, D_{30}, D_{50} are the grain sizes in (mm) at which 90, 30, and 50 percent respectively of the total weight is finer, D is the hydraulic depth of flow computed from Manning's equation for flow along the breach at any instant of time, S is the breach bottom slope which is assumed to always be parallel to the downstream face of the dam, P is the total perimeter of the breach, and τ_c is Shield's critical shear stress that must be exceeded before erosion occurs. The incremental increase in the breach bottom and sides (ΔH_c) which occurs over a very short interval of time is given by:

$$\Delta H_c = Q_s \Delta t / [P\ L\ (1-p)] \quad \text{.....(45)}$$

in which L is the length of the breach through the dam, and p is the porosity of the breach material.

Computational Algorithm

The sequence of computations in the model are iterative since the flow into the breach is dependent on the bottom elevation of the breach and its width while the breach dimensions are dependent on the sediment transport capacity of the breach flow and the sediment transport capacity is dependent on the breach size and flow. A simple iterative algorithm is used to account for the mutual dependence of the flow, erosion, and breach properties. An estimated incremental erosion depth ($\Delta H_c'$) is used at each time step to start the iterative solution. This estimated value can be extrapolated from previously computed values. Convergence is assumed when ΔH_c computed from Eq. (45) differs from $\Delta H_c'$ by an acceptable specified tolerance. Typical applications of the BREACH model require less than 2 minutes on microcomputers with a math coprocessor. The computations show very little sensitivity to a reasonable variation in the specified time step size. The model has displayed a lack of numerical instability or convergence problems.

Testing and Verification

BREACH was applied to the piping initiated failure of the Teton earthfill dam which breached in June 1976, releasing an estimated peak discharge of 2.3 million cfs (65,128 cms) having a range of 1.6 to 2.6 million cfs (45,450-73,860 cms). The simulated breach hydrograph is shown in Fig. 6. The computed final top breach width of the trapezoidal breach was 645 ft (213 m) compared to the observed width of 650 ft (214.7 m). The computed side slope of the breach was 1:1.06 compared to 1:1.00. Additional information on this

and another application of BREACH to the naturally formed landslide dam on the Mantaro River in Peru, which breached in June 1984, can be found elsewhere (Fread, 1984, 1987). The model has also been satisfactorily verified with the piping initiated failure of the 28 ft (8.5 m) high Lawn Lake dam in Colorado in 1982.

REFERENCES

1. Davidson, D. D., and B. L. McCartney, "Water Waves Generated by Landslides in Reservoirs," Journ. Hydraulics Div., ASCE, 101, HY12, pp. 1489-1501, Dec., 1975.

2. Davies, W. E., J. F. Baily, and D. B. Kelly, "West Virginia's Buffalo Creek Flood: A Study of the Hydrology and Engineering Geology," Geological Survey, Circular 667, U.S. Geological Survey, 32 pp, 1975.

3. DeLong, L. L., "Extension of the Unsteady One-Dimensional Open Channel Flow Equations for Flow Simulation in Meandering Channels with Flood Plains," Selected Papers in HydroScience, U.S. Geological Survey Water-Supply Paper 2220, pp. 101-105, 1985.

4. De Saint-Venant, Barre, "Theory of Unsteady Water Flow, with Application to River Floods and to Propagation of Tides in River Channels," Acad. Sci. (Paris) Comptes rendus, 73, pp. 237-240, 1871.

5. Fread, D. L., "A Technique for Implicit Flood Routing in Rivers with Major Tributaries," Water Resources Research, AGU, Vol. 9, No. 4, pp. 918-926, Aug., 1973.

6. Fread, D. L., "The Development and Testing of a Dam-Break Flood Forecasting Model," Proceedings, Dam-Break Flood Modeling Workshop, U.S. Water Resources Council, Washington, D.C., 32 pp, Oct. 18-20, 1977.

7. Fread, D. L., "NWS Operational Dynamic Wave Model," Verification of Math. and Physical Models in Hydraulic Engr., Proceedings: 26th Annual Hydr. Div., Spec. Conf., ASCE, College Park, Maryland, pp. 455-464, Aug., 1978.

8. Fread, D. L., "DAMBRK: The NWS Dam-Break Flood Forecasting Model," Hydrologic Research Laboratory, National Weather Service, Silver Spring, Maryland, 56 pp, 1984.

9. Fread, D. L., "A Breach Erosion Model for Earthen Dams," Proceedings of Specialty Conference on Delineation of Landslides, Flash Flood, and Debris Flow Hazards in Utah, Utah State University, 30 pp, June 15, 1984.

10. Fread, D. L., "Channel Routing," Hydrological Forecasting, (Editors: M. G. Anderson and T. P. Burt), Chapter 14, John Wiley and Sons, pp. 437-503, 1985.

11. Fread, D. L., "BREACH: An Erosion Model for Earthen Dam Failures," Hydrologic Research Laboratory, NOAA, NWS, U.S. Department of Commerce, Silver Spring, Maryland, June, 34 pp., 1987.

12. Fread, D. L., and T. E. Harbaugh, "Transient Hydraulic Simulation of Breached Earth Dams," Journal of the Hydraulics Division, American Society of Civil Engineers, Vol. 99, No. HY1, pp. 139-154, Jan., 1973.

13. Fread, D. L., and G. F. Smith, "Calibration Technique for 1-D Unsteady Flow Models," Journal of the Hydraulics Division, ASCE, Vol. 104, No. HY7, pp. 1027-1044, July, 1978.

14. Fread, D. L., and J. M. Lewis, "FLDWAV: A Generalized Flood Routing Model," ASCE, Proceedings of National Conference on Hydraulic Engineering, Colorado Springs, Colorado, 6 pp., 1988.

15. Froehlich, D. C., "Embankment-Dam Breach Parameters," Proceedings of the 1987 National Conference of Hydraulic Engineering, ASCE, New York, New York, pp. 570-75, Aug., 1987.

16. Johnson, F. A., and P. Illes, "A Classification of Dam Failures," Water Power and Dam Construction, pp. 43-45, Dec., 1976.

17. Koutitas, C. G., "Finite Element Approach to Waves Due to Landslides," Journ. Hydraulics Div., ASCE, 103, HY9, pp. 1021-1029, Sept., 1977.

18. Lin, J. O., and H. K. Soong, "Junction Losses in Open Channel Flows," Water Resources Research, AGU, Vol. 15, No. 2, pp. 414-418.

19. MacDonald, T. C., and J. Langridge-Monopolis, "Breaching Characteristics of Dam Failures," Journ. Hydraulics Div., ASCE, 110, No. 5, pp. 567-586, May, 1984.

20. Morris, H. M., and J. M. Wiggert, Applied Hydraulics in Engineering, The Ronald Press Co., New York, pp. 570-573, 1972.

21. Ray, H. A., L. C. Kjelstrom, E. G. Crosthwaite, and W. H. Low, "The Flood in Southeastern Idaho from Teton Dam Failure of June 5, 1976," Open File Report, U.S. Geological Survey, Boise, Idaho, 1976.

22. Singh, K. P., and A. Snorrason, "Sensitivity of Outflow Peaks and Flood Stages to the Selection of Dam Breach Parameters and Simulation Models, University of Illinois State Water Survey Division, Surface Water Section, Champaign, Illinois, 179 pp., June, 1982.

23. Smart, G. M., "Sediment Transport Formula for Steep Channels," Journal of Hydraulics Division, American Society of Civil Engineers, Vol. 110, No. 3, pp. 267-276, 1984.

24. Westphal, J. A., and D. B. Thompson, "NWS Dambreak or NWS Simplified Dam Breach," Computational Hydrology '87, H17-H23, Anaheim, California, 1987.

25. Wetmore, J. N., and D. L. Fread, "The NWS Simplified Dam Break Flood Forecasting Model for Desk-Top and Hand-Held Microcomputers," Printed and Distributed by the Federal Emergency Management Agency (FEMA), 122 pp., 1984.